Mitigation of Wind Turbine Clutter for Weather Radar by Signal Separation

Faruk Uysal, *Member, IEEE*, Ivan Selesnick, *Senior Member, IEEE*, and Bradley M. Isom, *Member, IEEE*

***Abstract*—This paper addresses the mitigation of wind turbine clutter (WTC) in weather radar data in order to increase the performance of existing weather radar systems and to improve weather analyses and forecasts. We propose a novel approach for this problem based on signal separation algorithms. We model the weather signal as group sparse in the time–frequency domain; in parallel, we model the WTC signal as having a sparse time derivative. In order to separate WTC and the desired weather returns, we formulate the signal separation problem as an optimization problem. The objective function to be minimized combines total variation regularization and time–frequency group sparsity. We also propose a three-window short-time Fourier transform for the time–frequency representation of the weather signal. To show the effectiveness of the proposed algorithm on weather radar systems, the method is applied to simulated and real data from the next-generation weather radar network. Significant improvements are observed in reflectivity, spectral width, and angular velocity estimates.**

***Index Terms*—Dynamic clutter mitigation, signal separation, sparse optimization, weather radar, wind turbine clutter (WTC).**

I. Introduction

THE demand for green energy has been increasing for over a decade. Wind is one of the fastest growing sources of electricity in many countries, and there are many new wind farm developments under construction. According to the American Wind Energy Association report [1], the United States has an installed wind capacity of 61 327 MW, and there are over 13 000 MW currently under construction.

A typical wind farm has several wind turbines, which consist of multiple stationary and moving components such as a tower, a nacelle, and blades. The height of the wind turbine's tower and blades may exceed 100 ft. The enormous size and motion of the blades create interference for radar systems. The unwanted radar return from wind farms, also known as *wind turbine clutter* (WTC), is considered to be dynamic clutter due to the nonzero Doppler return created by rotating wind turbine blades. These unwanted radar returns (interference) affect the critical operation of current radar systems. The impact of wind farms on different radar systems, such as air traffic control [2], [3], air surveillance radar [3]–[6], and weather radars [3], [7]–[9], are different. Radar returns from large radar targets are different than returns from distributed weather scatters. Moving targets are well localized in the Doppler domain [6], simplifying mitigation of WTC. However, weather returns span a wider spectrum and make signal discrimination challenging. These challenges and mitigation strategies for WTC in weather radar systems are discussed in various publications [3], [9]–[13].

Several approaches have been developed for the mitigation of WTC in weather radar data. Some methods, such as those based on spectral interpolation, are introduced in [9]–[12]. These methods aim to detect the contaminated radar data and substitute them with an estimate using (multidimensional) interpolation, where interpolation is applied to both the spectral moments and the spectral components. These methods treat the WTC mitigation problem as an estimation problem. In other words, these methods aim to replace the contaminated data with estimates from the uncontaminated data instead of directly mitigate the effects of WTC.

Another algorithm depends on adaptive spectrum processing [14]. In this approach, the mean radial velocity estimates from the uncontaminated volume around the contaminated region are used as an initial data pool to obtain the power spectral density (PSD) of the weather. These estimates are then used to filter the contaminated data.

It is known that, in order to increase the statistical credibility of the PSD estimate, more samples are needed from uncontaminated data. The same argument is also true for interpolation in that the success of these methods depends on the number of uncontaminated data samples and their Euclidean distance to the contaminated volume. The dependence on prior information (or uncontaminated data) is a major drawback for mitigation of large-scale wind farms where the wind turbines are located very close to each other. These methods are not effective at mitigating WTC in a data fragment such as the data shown in Fig. 1. The contaminated weather data shown in Fig. 1 are created by coherently adding the simulated weather data (Wx) and the cropped actual WTC data, where the weather signal to WTC signal power ratio $(10\log(P_{\mathrm{Wx}}/P_{\mathrm{WTC}}))$ is manually set to -25 dB for a controlled experiment (explained in detail in Section II).

Manuscript received June 11, 2015; revised October 19, 2015 and November 23, 2015; accepted November 26, 2015. Date of publication January 11, 2016; date of current version March 25, 2016. This work was supported in part by the Office of Naval Research under Grant N00014-15-1-2314.

F. Uysal is with the Advanced Radar Research Center, The University of Oklahoma, Norman, OK 73019 USA, and also with the Department of Electrical and Computer Engineering, Tandon School of Engineering, New York University, Brooklyn, NY 11201 USA (e-mail: faruk.uysal@ou.edu).

I. Selesnick is with the Department of Electrical and Computer Engineering, Tandon School of Engineering, New York University, Brooklyn, NY 11201 USA.

B. M. Isom is with Pacific Northwest National Laboratory, Richland, WA 99352 USA.

Color versions of one or more of the figures in this paper are available online at http://ieeexplore.ieee.org.

Digital Object Identifier 10.1109/TGRS.2015.2508380

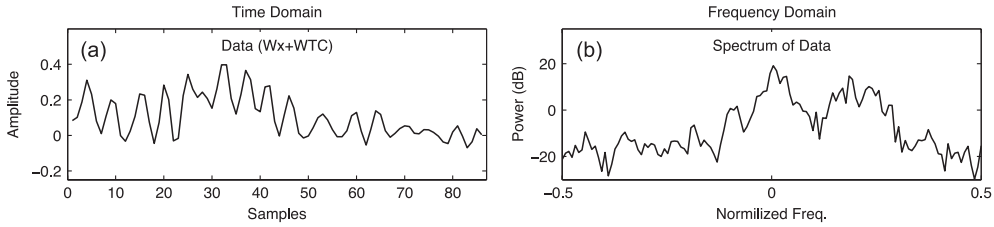

Fig. 1. Fragment of contaminated weather radar data samples. (a) Real part. (b) Spectrum.

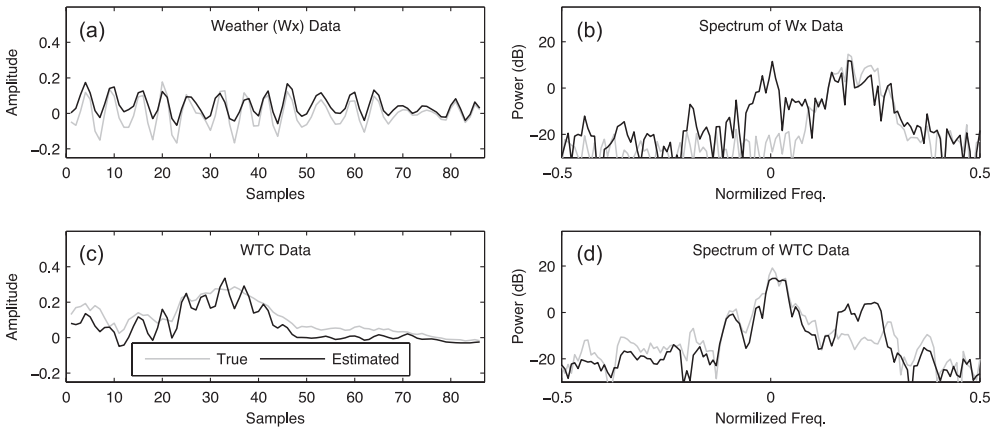

Fig. 2. Results of signal separation method proposed in [17]. (a) True and estimated weather data (real part) in time domain and (b) their spectrum. (c) True and estimated wind turbine data (real part) in time domain and (d) their spectrum.

Recently proposed signal separation techniques for radar applications aim to separate the given radar data into their components (such as static clutter, dynamic clutter, and target of interest), independent of prior or current radar data collected from different elevations, azimuth, and range cells [6], [15]–[18]. A sparsity-based dynamic clutter mitigation technique introduced in [17] is applied to contaminated weather data shown in Fig. 1, to extract the weather and WTC components. Fig. 2 depicts the results of the signal separation method proposed in [17]. The mean square error (MSE) for the separated components of this example was computed as 48×10^{-4}. As shown in Fig. 2, the result of signal separation is not satisfactory, due to the fact that the method introduced in [17] is designed under two assumptions. First, the target of interest is assumed to be high-radar-cross-section (RCS) moving targets. Second, coherent processing interval is long enough to capture the features of WTC (radar operates in a side-looking mode). Note that, for weather radar, these assumptions are not valid because weather has a low RCS and is spread over a large spectrum compared with the typical hard radar targets (such as an airplane). In addition, the coherent processing interval is limited to 100 samples, which makes WTC features unresolvable.

The method proposed in this paper is not dependent on any prior data. We introduce a novel lossless signal separation algorithm to approximately recover the WTC and weather signal from contaminated radar data sets by minimizing a proposed objective function. In Section II, we investigate the features of weather and WTC for a weather radar operating in the traditional scan mode. We model the weather signal as being group sparse in the spectral domain and the WTC signal as having a sparse time derivative. The objective function is defined in Section III as a combination of total variation (TV) and group sparse regularization in order to achieve weather radar signal separation. The application of the proposed algorithm to real weather radar data sets and the inherent implications for weather forecasting are discussed in Section IV. Finally, the advantages and disadvantages of the proposed method versus several previously developed algorithms are discussed in Section V.

II. WTC and Weather

Wind turbines consist of several main components, namely, the rotary blades, the nacelle, and the tower. Radar returns from the tower and nacelle of the wind turbine have similar properties to ground clutter due to their stationarity (zero Doppler velocity). Either classic ground clutter filters in the time domain [19] or advanced filters in the spectral domain [20] can be utilized to mitigate stationary ground clutter. The radar returns from the turbine rotary blades are classified as dynamic clutter, and ground clutter filters are ineffective at mitigating the dynamic WTC while preserving weather returns. The micro-Doppler signature of the wind turbines and the clutter contamination show differences according to radar type and operation mode. The WTC can be modeled theoretically for the side-looking mode where the radar antenna is fixed during the collection. In side-looking mode, periodic flashes occur and are observable in the Doppler spectrum when the blades are in a vertical position (perpendicular to the line of sight of radar) [6], [9], [13], [17]. In scan mode, the micro-Doppler signature of wind turbines

is not easily resolvable due to the limited coherent processing interval. In fact, the WTC spectrum appears similar to that of a noise signal combined with a strong zero Doppler return.

The spectrum of weather data varies as a function of precipitation. Weather signals are usually characterized by their mean velocity, spectrum width, and power density [21]. In general, weather data are modeled using a Gaussian-like PSD [14], [21]. In order to establish a controlled experiment, weather data with a 10-m/s mean velocity and a 1.5-m/s spectrum width were simulated as described in [21]. Simulation parameters are selected according to the real operating conditions of the Next Generation Radar (NEXRAD) volume coverage patterns 21 (VCP-21) 0.5° contiguous Doppler scan as described in [22]. In this case, the scan has a pulse repetition frequency of 1014 Hz and collects approximately 89 pulses per azimuth bin. The Nyquist velocity is 26.2 m/s, creating a spectral resolution of approximately 0.6 m/s. The real part of the simulated weather signal is shown in Fig. 2(a), and its spectrum is depicted in Fig. 2(b) (gray solid line). Unlike weather radar data, simulation of WTC depends on many specific factors such as blades' position and rotation rate. Generating quality synthetic WTC data for a weather radar operating in scan mode requires a statistical simulation using measured WTC data as a basis [11]. To make our controlled experiment more realistic, we use WTC data that are cropped from a real weather radar data set (explained in detail in Section IV-A). The real component of the WTC data is shown in Fig. 2(c), and its spectrum is shown in Fig. 2(d), respectively.

III. Signal Separation Algorithm for Weather Radar

This paper aims to develop an approach for WTC mitigation in weather radar data based on signal separation algorithms. Consider the generic signal separation problem where an observed signal $\mathbf{y} \in \mathbb{C}^N$ is to be modeled as the sum of two component signals $\mathbf{x}_1$ and $\mathbf{x}_2$, shown as

$$\mathbf{y} = \mathbf{x}_1 + \mathbf{x}_2. \tag{1}$$

The recovery of $\mathbf{x}_i$ (where $i = 1, 2$) from $\mathbf{y}$ is ill conditioned in that there are infinitely many solutions. One may choose to set $\mathbf{x}_1$ arbitrarily and set $\mathbf{x}_2 = \mathbf{y} - \mathbf{x}_1$. The estimation of $\mathbf{x}_i$ from $\mathbf{y}$ can be only meaningfully performed when $\mathbf{x}_i$ and $\mathbf{y}$ have distinct properties and when these properties are known or approximately known. Furthermore, $\mathbf{x}_i$ should be sufficiently distinct from $\mathbf{y}$ to make the problem meaningful.

The morphological component analysis (MCA) approach assumes that two component signals allow sparse representations with respect to distinct transforms $\mathbf{F}_1$ and $\mathbf{F}_2$, respectively [23]. One formulation of MCA aims to find the coefficients $\mathbf{a}_i$ with respect to the transform $\mathbf{F}_i$. In this formulation, the component signals are represented (synthesized) in terms of the coefficients, shown as

$$\mathbf{x}_1 = \mathbf{F}_1\mathbf{a}_1, \quad \mathbf{x}_2 = \mathbf{F}_2\mathbf{a}_2. \tag{2}$$

Therefore, instead of finding $\mathbf{x}_1$ and $\mathbf{x}_2$ such that $\mathbf{y} = \mathbf{x}_1 + \mathbf{x}_2$, this formulation of MCA seeks coefficients $\mathbf{a}_1$ and $\mathbf{a}_2$ such that

$$\mathbf{y} = \mathbf{F}_1\mathbf{a}_1 + \mathbf{F}_2\mathbf{a}_2. \tag{3}$$

Similar to the problem shown in (1), this problem is also ill conditioned. To find a particular solution, MCA follows a variational framework and minimizes a predetermined cost function chosen to promote sparsity of $\mathbf{a}_i$. Once the optimal coefficients $\hat{\mathbf{a}}_1$ and $\hat{\mathbf{a}}_2$ are obtained, MCA estimates the components as

$$\hat{\mathbf{x}}_1 = \mathbf{F}_1\,\hat{\mathbf{a}}_1, \quad \hat{\mathbf{x}}_2 = \mathbf{F}_2\,\hat{\mathbf{a}}_2. \tag{4}$$

To find the optimal coefficients $\hat{\mathbf{a}}_i$, one may consider a ℓ_1-norm approach, which can be shown as

$$\{\hat{\mathbf{a}}_1, \hat{\mathbf{a}}_2\} = \arg\min_{\mathbf{a}_1,\,\mathbf{a}_2} \ \|\mathbf{a}_1\|_1 + \|\mathbf{a}_2\|_1 \tag{5a}$$

$$\text{such that} \ \ \mathbf{y} = \mathbf{F}_1\mathbf{a}_1 + \mathbf{F}_2\mathbf{a}_2. \tag{5b}$$

In order to apply MCA framework to WTC mitigation problem, we assumed that the contaminated radar data $\mathbf{y}$ can be modeled as

$$\mathbf{y} = \mathbf{a}_1 + \mathbf{F}_2\mathbf{a}_2 \tag{6}$$

where $\mathbf{a}_1$ represents the WTC data ($\mathbf{F}_1 = \mathbf{I}$), and $\mathbf{F}_2\mathbf{a}_2$ represents the weather data. The weather data coefficient in the transform domain $\mathbf{F}_2$ (inverse transform) is denoted by $\mathbf{a}_2$. This time, the weather signals with a Gaussian-like PSD are assumed to have a group sparse property in frequency or time–frequency domain. Note that, a group sparse signal is one where large magnitude signal values tend not to be isolated; instead, these large magnitude values tend to form groups [24]. Furthermore, it is assumed that the WTC signal has a sparse time derivative. Unlike weather signals, due to the fast dynamic behavior of the wind turbines, the power spectrum of WTC changes scan to scan. Although WTC generates strong returns around the low frequencies, there are also significant returns in the high-frequency components. It is reasonable to treat time series WTC signals as noise for weather radar systems operating in scan mode.

The convex regularization is a standard approach in sparse signal processing. The TV is widely used as a regularizer when the derivative of the input signal is known to be sparse or approximately sparse. The TV, which is the ℓ_1-norm of the derivative, is defined as [25], [26]

$$\mathrm{TV}(x) = \sum_n |x(n+1) - x(n)|\,. \tag{7}$$

The ℓ_1-norm and other separable sparsity models do not capture the tendency of coefficients to cluster (group sparsity). An approach, i.e., overlapping group shrinkage (OGS), based on the minimization of a convex cost function incorporating a mixed norm is introduced in the literature [24]. In this approach, the groups are fully overlapping so that the denoising method is shift invariant and blocking artifacts are avoided. Furthermore, it is not assumed that the group locations are known (in this context, radial velocity), nor that the group boundaries are known (in this context, spectral width). The group sparsity

TABLE I
SIGNAL SEPARATION ALGORITHM FOR WEATHER RADAR

Input : $\mathbf{y}$

Initialize: $\mathbf{F}_1 = \mathbf{I}$, $\mathbf{F}_2 = \text{STFT}$, $\mathbf{d}_i \geq 0$, for $i = 1, 2$

1: $\mathbf{v}_1 \leftarrow \text{TVD}(\mathbf{a}_1 + \mathbf{d}_1, \lambda_1/\mu) - \mathbf{d}_1$
2: $\mathbf{v}_2 \leftarrow \text{OGS}(\mathbf{a}_2 + \mathbf{d}_2, \lambda_2/\mu, K) - \mathbf{d}_2$
3: $\mathbf{c} \leftarrow \mathbf{y} - \mathbf{F}_1\mathbf{v}_1 - \mathbf{F}_2\mathbf{v}_2$
4: $\mathbf{d}_i \leftarrow \frac{1}{2}\mathbf{F}_i^{\mathsf{H}}\mathbf{c}$
5: $\mathbf{a}_i \leftarrow \mathbf{d}_i + \mathbf{v}_i$

Repeat until convergence

* TVD and OGS are available on-line at
http://eeweb.poly.edu/iselesni/software/

inducing norm has been used previously to exploit overlapping clustering of sparsity in [24] and [27]–[29] and may be defined as

$$G(x) = \sum_n \left[\sum_k^{K-1} |x(n+k)|^2 \right]^{\frac{1}{2}}. \tag{8}$$

We use the TV (7) and overlapping group sparsity promoting penalty function (8) as the regularizer to separate the two signals. The optimization problem for WTC and weather signal separation is defined as

$$\min_{\mathbf{a}_1,\, \mathbf{a}_2} \quad \lambda_1 \text{TV}(\mathbf{a}_1) + \lambda_2 G(\mathbf{a}_2) \tag{9a}$$

$$\text{such that:} \quad \mathbf{a}_1 + \mathbf{F}_2\mathbf{a}_2 = \mathbf{y}. \tag{9b}$$

The terms λ_i are the regularization parameters, and K is the group size for the group sparse signal. Note that K does not define the exact group size (spectral width of the weather spectrum). When the group size is greater than one sample ($K > 1$), the groups overlap, and every element of the solution depends on every element of the input signal [24]. The solution of the optimization problem (9) can be achieved iteratively using the split augmented Lagrangian shrinkage algorithm (SALSA), as shown in Table I (see the Appendix for details).

STFT: We propose a three-window short-time Fourier transform (STFT) as the transform $\mathbf{F}_2$ for the time–frequency representation of the time-varying radar signature of WTC. We apply three different weighting windows to the time series signal, corresponding with the beginning, middle, and end. The three-window STFT for a length N input signal $\mathbf{x}$ is defined as

$$X_j(\omega) = \mathcal{F}\{x(n) w_j(n)\} \tag{10}$$

where w_j is the window function ($j = 1, 2, 3$). We select the power-of-cosine function

$$\cos^{\alpha}\left(\frac{\pi n}{(N-1)} - \frac{\pi}{2}\right) \tag{11}$$

as a template to design the three windows due to its flexibility. The rectangular window function ($\alpha = 0$), the cosine window function ($\alpha = 1$), and the Hann window function ($\alpha = 2$) are known special cases of this window function. The N-point first half cycle of the power-of-cosine function is selected as the first window function, given by

$$w_1(n) = \cos^{\alpha}\left(\frac{\pi n}{(2N-1)} - \frac{\pi}{2}\right). \tag{12}$$

Similarly, the N-point second half cycle of the power-of-cosine function is selected as a complement to the first window function w_1, given by

$$w_3(n) = \cos^{\alpha}\left(\frac{\pi(N-1-n)}{(2N-1)} - \frac{\pi}{2}\right). \tag{13}$$

The actual power-of-cosine window is length $2N$, and a half cycle is length N. The final window function is chosen to enforce the perfect reconstruction property $(w_1{}^2(n) + w_2{}^2(n) + w_3{}^2(n) = 1)$ [30] and is given by

$$w_2(n) = \sqrt{1 - w_1{}^2(n) + w_3{}^2(n)}. \tag{14}$$

The window functions for $\alpha = 2$ are illustrated in Fig. 3. The inverse transform of the three-window STFT defined in (10) is given by

$$x(n) = \sum_j \mathcal{F}^{-1}\{X_j(\omega)\} w_j(n). \tag{15}$$

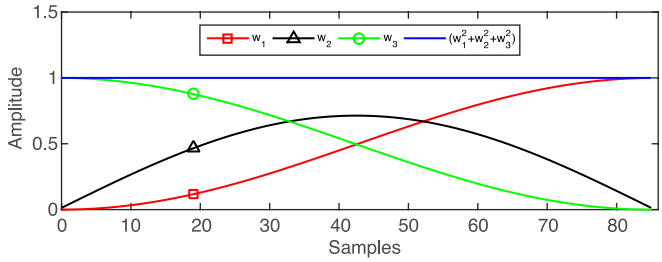

Fig. 3. Window functions of STFT.

IV. RESULTS

The proposed method was applied to the simulated data shown in Fig. 1 to demonstrate the separation of weather and WTC signals. The algorithm parameters were adjusted manually to obtain the best results. The relative values of λ_1 and λ_2 in (9) influence the energy of the two signal components, and without loss of generality, we set

$$\lambda_2 = 1 - \lambda_1. \tag{16}$$

Hence, there is a single regularization parameter $0 \leq \lambda_1 \leq 1$. For processing the simulated data, λ_1 was selected as 0.025, the algorithm parameter μ was set to 250, and the number of iterations was set to 200. Note that the coefficients in the STFT domain $\mathbf{a}_2$ are two dimensional (3 by N). Therefore, the group sparsity problem must be solved in 2-D space. The 2-D group size was selected as $K_1 = 3$ and $K_2 = 20$ for the simulated signal. (For M-dimensional space, the group size would be defined as $K = (K_1, K_2, \ldots, K_M)$).

Simulation results show that the proposed algorithm is promising to separate the mixed weather and wind turbine

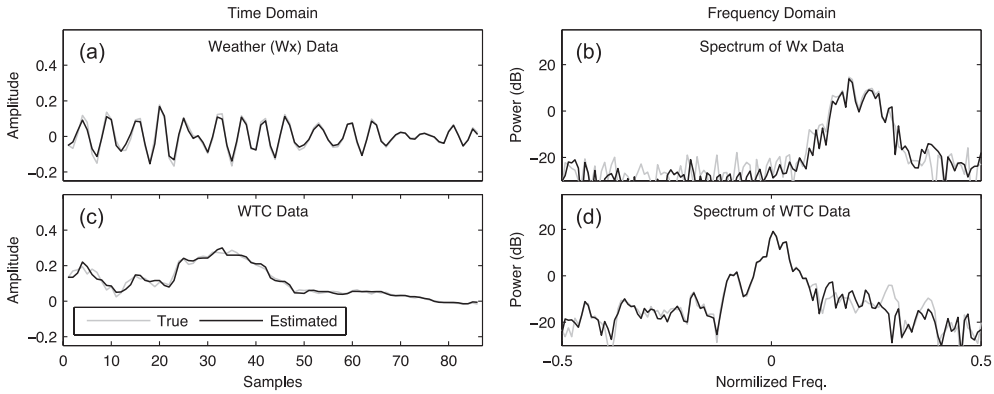

Fig. 4. Results of the proposed signal separation algorithm: (a) True and estimated weather data (real part) in time domain and (b) their spectrum. (c) True and estimated wind turbine data (real part) in time domain and (d) their spectrum.

radar signals. Fig. 4(a) and (b) illustrates the true (gray) and recovered (black) signals in time and frequency domains, respectively. Similarly, the true and recovered WTC signals are shown in the time and frequency domains in Fig. 4(c) and (d), respectively. As seen from the spectrum plots, the algorithm exhibits particularly high accuracy in the regions containing strong spectral moments. For the proposed method, the MSE of recovered weather signal was computed as 4.7×10^{-4}. Once again, the MSE for the recovered time samples was computed as 48×10^{-4} for the results shown in Fig. 2 (results of the sparsity-based dynamic clutter mitigation technique introduced in [17]).[1]

A. Weather Radar Data

Due to the lack of known ground truth, a controlled experiment data set was created to evaluate the success of the algorithm by using KDDC data, similar to [9], [12], [14], and [31]. The WSR-88D Level-I radar data were collected using a Sigmet RVP8 digital receiver at Dodge City, Kansas (KDDC), in 2006. The WTC was present due to the Gray County wind farm located southwest of the radar site. The weather data were collected from an isolated storm at the same range and time located northeast of the radar site. The IQ data from the wind farm were coherently added to the weather signals to generate contaminated weather data. Note that the data introduced were collected in scan mode and are displayed in plan position indicator format, as shown in Fig. 7.

The proposed separation algorithm can be applied to radar data both with and without WTC for different purposes. The method can be applied to the contaminated range bins to separate the weather and WTC for the purpose of WTC mitigation. Moreover, it can be applied to the uncontaminated range bins to mitigate (separate) the ground clutter.

To apply the algorithm, a first step is to classify each range bin as contaminated or uncontaminated. In most cases, wind farm locations are known or can be discovered through public wind farm location maps. It is also possible to use an automatic WTC detection algorithm to identify the contaminated range bins [32], although we do not use this technique.

[1]Note that MSE is only conclusively valid when the weather signal is not contaminated by ground clutter. Thus, MSE metric is only used to compare the results of simulated data sets.

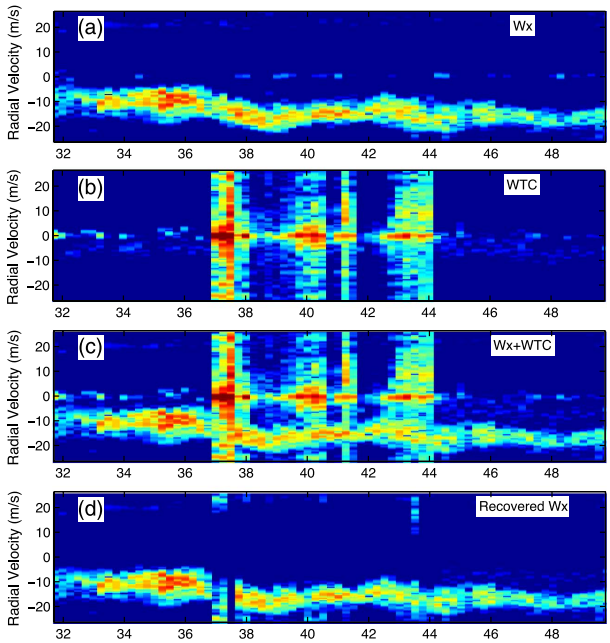

Fig. 5. Range-Doppler map azimuth 243° and elevation 0.4834°. (a) True weather data. (b) True WTC data. (c) Contaminated (mixed) data. (d) Recovered weather data after process. (e) Recovered wind turbine data after process.

The optimum values of λ_1 and λ_2 are data dependent and need to be selected based on the task at hand. For this particular data set, we adjust the algorithm parameters empirically to achieve the best result as follows: the regularization parameter λ_1 was set to 0.04 for the contaminated range bins and was set to 0.02 elsewhere. The number of iterations was set to 200, and μ was set to 250. The group size for the weather spectrum was selected as $K_1 = 3$ and $K_2 = 20$, same to the simulation. It was observed that the cost function converged after 100 iterations.

In order to separate the weather and the clutter (both static and dynamic), the proposed method was applied individually to time series signals that were collected at each time, azimuth, elevation, and range bin. Fig. 5 shows the range-Doppler map of the data from KDDC at azimuth 243° and elevation 0.4834° on March 30, 2006 at 20:34:17. The range-Doppler maps of the actual weather and WTC are shown in Fig. 5(a) and (b),

respectively. The location of wind turbines is easily recognizable, spanning the range of 37–44 km with elevated Doppler returns across the entire spectrum. The contaminated radar returns are shown in Fig. 5(c). The results of the proposed algorithm are depicted in Fig. 5(d) and (e). Note that the actual weather signal has ground clutter returns present [see Fig. 5(a)], whereas the recovered weather signal does not contain any clutter returns, except the residuals from the wind turbines [see Fig. 5(d)]. The algorithm cannot fully recover the actual input signal, but the recovered clutter-free weather data are still more desirable for weather applications. The separated static (ground) clutter is combined with the dynamic WTC and is shown in Fig. 5(d). The separation process is fully reversible, and the original contaminated signal can be recovered by the summation of the two signal components.

Dual-polarization capabilities were not available on the NEXRAD systems in 2006 when the data used here were collected. As such, the analysis focuses on the three primary weather radar variables: power, radial velocity, and spectrum width. Each of these three variables plays a significant role in understanding and predicting weather events and can be harmfully biased by WTC. The power estimate, after conversion to reflectivity, provides information about the nature of the hydrometeors, including size and number, which can be used in downstream algorithms to determine important quantities such as rainfall rate. The radial velocity (first moment) estimator provides valuable information regarding wind speed and direction, which is used to identify downbursts and mesocyclones. The spectrum width estimator provides information about turbulence and velocity dispersion within the resolution volume. The power and radial velocity ν estimates are calculated from

$$P = 10\log 10\left(\frac{1}{N}\sum\left|x(n)^2\right|\right) \tag{17}$$

$$\nu = -\frac{\lambda}{4\pi T_s}\angle R(1) \tag{18}$$

where T_s is the pulse repetition time, and $\angle R(1)$ is the phase of first lag of the autocorrelation function. The estimators from (17) and (18) were selected due to their use in the NEXRAD weather radars (see [33] and [34]). Traditionally, clutter filtering is performed prior to moment estimation either through an elliptic filter or an adaptive spectral filter, with the goal of removing the DC signal with minimal bias to the remaining spectral bins. In this case, the new methodology was used in lieu of traditional ground clutter filters, but the traditional weather radar moment estimators were retained. The spectrum width calculation is accomplished through a hybrid technique developed by NCAR 09 and uses multiple lags to achieve improved accuracy for narrow spectrum widths [35]. Reflectivity (dBZ) is a nondimensional unit of radar reflectivity which represents a logarithmic power ratio (in decibels, or dB) with respect to radar reflectivity factor Z [36]. Reflectivity is often used in meteorology (weather radar) and helps to determine the type of precipitation together with other variables analyzed from the radar returns.

Fig. 6 shows the spectrum width, radial velocity, and reflectivity estimation of the actual (red), contaminated (blue), and recovered (green) weather data shown in Fig. 5. Note that each

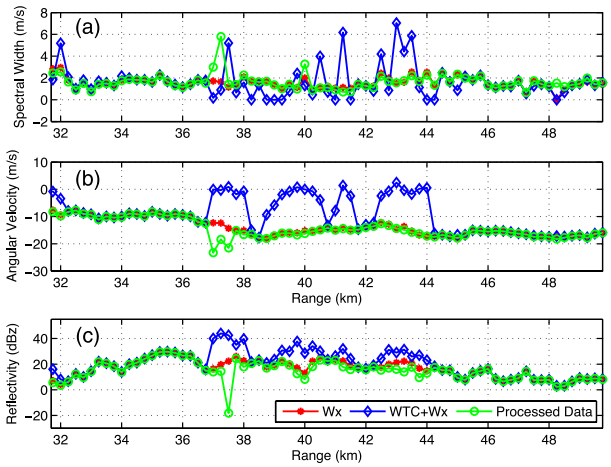

Fig. 6. Range versus (a) spectral width, (b) angular velocity, and (c) reflectivity of the weather data (azimuth 243° and elevation 0.4834°) for true, contaminated, and recovered weather data.

of the variables is biased by the presence of WTC. The proposed method is able to improve the estimation results of spectrum width, radial velocity, and reflectivity for most of the range bins, except three range bins between 37 and 38 km. The proposed method has difficulties in separating the signal components for these three range bins (see Fig. 5); thus, the estimation of weather-related parameters is not accurate for those range bins. Our investigations show that the actual weather to WTC power ratio for those range bins is too low $(10\log(P_{\mathrm{Wx}}/P_{\mathrm{WTC}}) < -25$ dB) to separate the signal components using the selected algorithm parameters. Note that the algorithm parameters are adjusted to optimize processing data over to the entire area of interest and are not individually adjusted for each range bin.

In Fig. 7(a)–(c), the reflectivity of the true weather, contaminated weather, and recovered weather data, respectively, from KDDC (March 30, 2006 at 20:34:17) at elevation 0.4834° is shown for the area of interest. Similarly, Fig. 7(d)–(f) shows the radial velocity estimation of the true weather, contaminated weather, and recovered weather data, respectively. Similar to the spectral plots in Fig. 5, the bias imposed by the WTC is evident. The reflectivity plots display elevated values in the WTC contaminated region, whereas the radial velocity plots show a bias toward zero due to the stationary clutter of the wind turbine tower (for more detailed information regarding the locations of the wind turbines, please refer to [31]). Following the application of the proposed method, much of the impact of the WTC was removed. Qualitatively, some biases are still evident, such as the red cell located at approximately $(-37, -15)$ in Fig. 7(f) or the elevated reflectivity located at $(-33, -13)$ in Fig. 7(c). Many of the significant differences are in areas of low return power or SNR along the northern edge of the area of interest, and these measurements would likely be censored.

V. Comparison With Previous Methods

As discussed in Section I, different methods have been introduced in the literature for WTC mitigation. However, not all proposed mitigation methods are able to achieve time-domain results comparable with the proposed method. For instance,

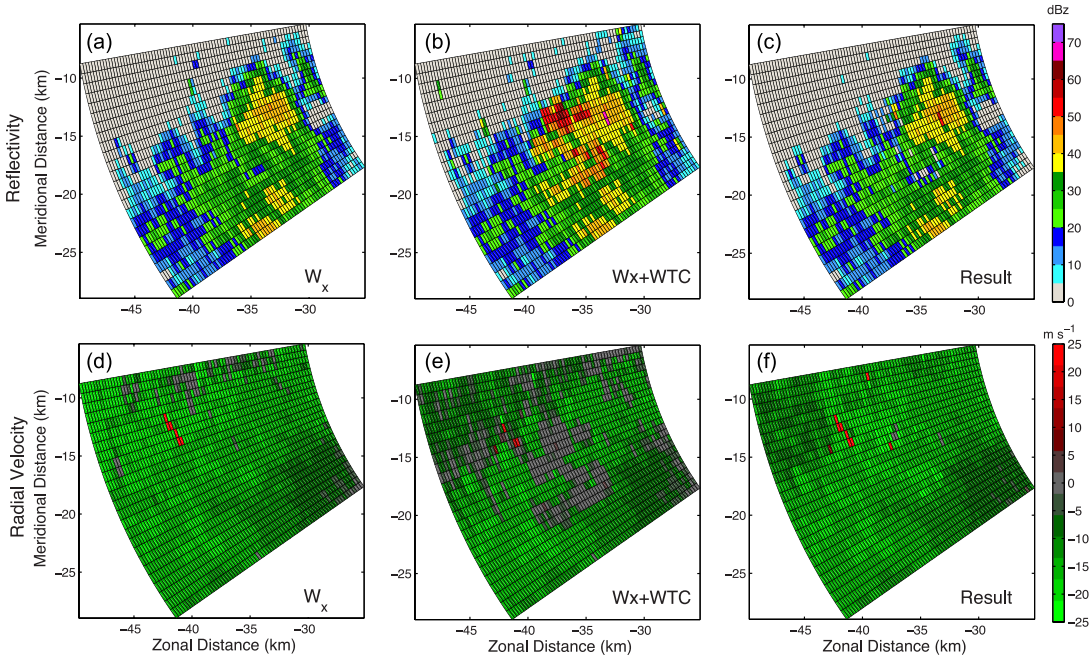

Fig. 7. Weather data from KDDC VCP 21 (March 30, 2006 at 20:34:17) at elevation 0.4834°. (a) Reflectivity of the true weather. (b) Reflectivity of WTC contaminated weather. (c) Reflectivity of recovered weather data. (d) Radial velocity of the true weather. (e) Radial velocity of WTC contaminated weather. (f) Radial velocity of recovered weather data.

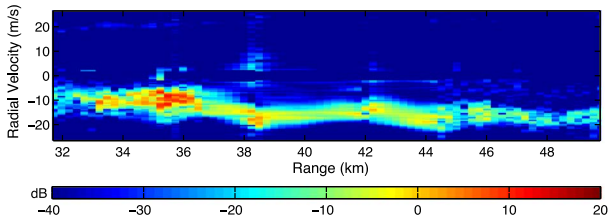

Fig. 8. Range-Doppler plot of 3-D spectral interpolation technique with a spectral clutter filter (proposed in [9]).

spectral interpolation techniques [9]–[12] are ineffective at producing time-domain estimates of weather radar data. Fig. 8 shows the range-Doppler plot resulting from the 3-D spectral interpolation technique with a spectral clutter filter (proposed in [9]). Comparing Fig. 5(d) with Fig. 8, it is observed that computing the range-Doppler map from processed time-domain samples (the proposed method) gives better results than spectral domain interpolation. For instance, for ranges between 40 and 42 km, the proposed method is able to preserve more details compared with the spectral interpolation method. In addition, some residuals are observed around 38 km after spectral clutter filtering and interpolation, whereas the proposed method achieves better clutter cancellation in the same region. As noted earlier, the proposed method fails at three range bins around range 37 km due to low SNR, and only for these three range bins does the 3-D spectral interpolation give better results. For future work, we are planning to investigate the results of concatenating these two methods. The proposed method would be used for clutter cancellation and WTC mitigation; then, an appropriate spectral interpolation method would be used to improve the final results.

VI. Conclusion

This paper has considered the problem of WTC mitigation in weather radar data for the purpose of improving the quality of forecasts and the performance of existing radar systems. The technique successfully recovers (except very low SNR cases) the weather signal component from data that are contaminated by nontraditional WTC. The signal separation algorithm is formulated as an optimization problem by defining a novel cost function that incorporates both time–frequency group sparsity and TV regularization. A three-window STFT is proposed as the time–frequency transform to capture changes on local sections of the signal. The fast-converging SALSA is used to minimize the cost function by dividing the complex optimization problem into simpler suboptimization problems.

The approach was validated using simulations and real experimental data collected using the WSR-88D KDDC at Dodge City, Kansas. The proposed algorithm was used on real data for two purposes: WTC mitigation on contaminated range bins and ground clutter mitigation for everywhere else. The results show that the proposed signal separation algorithm is a promising approach for mitigating WTC, thus helping to improve weather analyses and forecasts. The adaptive selection of algorithm parameters for optimization is still an active research topic and requires further investigation.

Appendix

Signal Notation: We denote the finite-length discrete signals by bold lower case letters. The N-point signal is written as

$$\mathbf{x} = [x(0), \ldots, x(N-1)]\,. \tag{19}$$

The (transform) matrices are denoted by bold upper case letters (i.e., $\mathbf{F}$), and functions are denoted by regular upper case letters, i.e., $R(\cdot)$. The ℓ_2-norm of a vector $\mathbf{x}$ is given as

$$\|\mathbf{x}\|_2 = \sqrt{\sum_n |\mathbf{x}(n)|^2}. \tag{20}$$

Derivation of the Algorithm: Consider the constrained minimization problem

$$\arg\min_{\mathbf{a}_1,\mathbf{a}_2} \quad \lambda_1\, R_1(\mathbf{a}_1) + \lambda_2\, R_2(\mathbf{a}_2) \tag{21a}$$

$$\text{such that} \quad \mathbf{F}_1\mathbf{a}_1 + \mathbf{F}_2\mathbf{a}_2 = \mathbf{y} \tag{21b}$$

where both $R_1(\cdot)$ and $R_2(\cdot)$ are convex functions. To solve this optimization problem, we use the SALSA [37], which is based on the alternating direction method of multipliers (ADMM) [38]. Note that proximal splitting methods, such as a Douglas–Rachford approach, could be also used to solve this problem [39].

The first step of SALSA is applying variable splitting by introducing the auxiliary variable $\mathbf{u}$ to obtain

$$\arg\min_{\mathbf{a}_1,\mathbf{a}_2,\mathbf{u}_1\mathbf{u}_2} \quad \lambda_1\, R_1(\mathbf{u}_1) + \lambda_2\, R_2(\mathbf{u}_2) \tag{22a}$$

$$\text{such that:} \quad \mathbf{F}_1\mathbf{a}_1 + \mathbf{F}_2\mathbf{a}_2 = \mathbf{y} \tag{22b}$$

$$\mathbf{u}_1 - \mathbf{a}_1 = 0 \tag{22c}$$

$$\mathbf{u}_2 - \mathbf{a}_2 = 0. \tag{22d}$$

The optimization problem (22) can be solved iteratively by applying the ADMM method, as shown in the following.

Initialize: $\mu > 0$, $\mathbf{d}_i$, $i = 1, 2$
Repeat

$$\mathbf{a}_i, \mathbf{u}_i \leftarrow \begin{cases} \arg\min_{\mathbf{a}_i,\mathbf{u}_i} \lambda_1\, R_1(\mathbf{u}_1) + \lambda_2\, R_2(\mathbf{u}_2) \\ \quad + \mu_1\, \|\mathbf{u}_1 - \mathbf{a}_1 - \mathbf{d}_1\|_2^2 + \mu_2\, \|\mathbf{u}_2 - \mathbf{a}_2 - \mathbf{d}_2\|_2^2 \\ \text{st: } \mathbf{F}_1\mathbf{a}_1 + \mathbf{F}_2\mathbf{a}_2 = \mathbf{y} \end{cases} \tag{23a}$$

$$\mathbf{d}_i \leftarrow \mathbf{d}_i - (\mathbf{u}_i - \mathbf{a}_i) \tag{23b}$$

Until convergence.

The vector $\mathbf{d}$ must be initialized prior to the iteration step, and the algorithm parameters μ_i must be user-selected positive scalars. The values of μ_i do not affect the solution to which the algorithm converges, but they do affect the convergence rate.

By alternately minimizing with respect to $\mathbf{a}$ and $\mathbf{u}$, we obtain the following algorithm.

Initialize: $\mu > 0$, $\mathbf{d}_i$, $i = 1, 2$
Repeat

$$\mathbf{u}_1, \mathbf{u}_2 \leftarrow \arg\min_{\mathbf{u}_1,\mathbf{u}_2} \lambda_1\, R_1(\mathbf{u}_1) + \lambda_2\, R_2(\mathbf{u}_2) + \mu_1\, \|\mathbf{u}_1 - \mathbf{a}_1 - \mathbf{d}_1\|_2^2 + \mu_2\, \|\mathbf{u}_2 - \mathbf{a}_2 - \mathbf{d}_2\|_2^2 \tag{24a}$$

$$\mathbf{a}_1, \mathbf{a}_2 \leftarrow \begin{cases} \arg\min_{\mathbf{a}_1,\mathbf{a}_2} \mu_1 \|\mathbf{u}_1 - \mathbf{a}_1 - \mathbf{d}_1\|_2^2 + \mu_2 \|\mathbf{u}_2 - \mathbf{a}_2 - \mathbf{d}_2\|_2^2 \\ \qquad \text{st: } \mathbf{F}_1\mathbf{a}_1 + \mathbf{F}_2\mathbf{a}_2 = \mathbf{y} \end{cases} \tag{24b}$$

$$\mathbf{d}_i \leftarrow \mathbf{d}_i - (\mathbf{u}_i - \mathbf{a}_i), \quad i = 1, 2. \tag{24c}$$

Until convergence.

Note that $\mathbf{u}_1$ and $\mathbf{u}_2$ are decoupled in (24a); thus, it can be written as

$$\mathbf{u}_i \leftarrow \arg\min_{\mathbf{u}_i} \lambda_i\, R_i(\mathbf{u}_i) + \mu_i\, \|\mathbf{u}_i - \mathbf{a}_i - \mathbf{d}_i\|_2^2. \tag{25}$$

If we assume that $\mathbf{F}_i$ is a tight frame, i.e., it satisfies the property $\mathbf{F}_i\mathbf{F}_i^{\mathsf{H}} = \mathbf{I}$ for $i = 1, 2$, then the solution of (24b)

$$\arg\min_{\mathbf{a}_1,\mathbf{a}_2} \quad \mu_1\, \|\mathbf{u}_1 - \mathbf{a}_1 - \mathbf{d}_1\|_2^2 + \mu_2\, \|\mathbf{u}_2 - \mathbf{a}_2 - \mathbf{d}_2\|_2^2 \tag{26}$$

$$\text{st:} \quad \mathbf{F}_1\mathbf{a}_1 + \mathbf{F}_2\mathbf{a}_2 = \mathbf{y} \tag{27}$$

is given explicitly by

$$\mathbf{a}_i = (\mathbf{u}_i - \mathbf{d}_i) + \frac{1}{\mu_i}\left(\frac{1}{\mu_1} + \frac{1}{\mu_2}\right)^{-1} \times \mathbf{F}_i^{\mathsf{H}}\left(\mathbf{y} - \mathbf{F}_1(\mathbf{u}_1 - \mathbf{d}_1) - \mathbf{F}_2(\mathbf{u}_2 - \mathbf{d}_2)\right). \tag{28}$$

Because μ_i is independent of the solution, it is convenient to set $\mu_1 = \mu_2 = \mu$. The resulting iterative algorithm can be written as follows.

Initialize: $\mu > 0$, $\mathbf{d}_i$, $i = 1, 2$
Repeat

$$\mathbf{u}_i \leftarrow \arg\min_{\mathbf{u}_i} \lambda_i R_i(\mathbf{u}_i) + \mu\|\mathbf{u}_i - \mathbf{a}_i - \mathbf{d}_i\|_2^2 \quad i = 1, 2 \tag{29a}$$

$$\mathbf{c} \leftarrow \mathbf{y} - \mathbf{F}_1(\mathbf{u}_1 - \mathbf{d}_1) - \mathbf{F}_2(\mathbf{u}_2 - \mathbf{d}_2) \tag{29b}$$

$$\mathbf{a}_i \leftarrow (\mathbf{u}_i - \mathbf{d}_i) + \frac{1}{2}\mathbf{F}_i^{\mathsf{H}}\mathbf{c} \qquad i = 1, 2 \tag{29c}$$

$$\mathbf{d}_i \leftarrow \mathbf{d}_i - (\mathbf{u}_i - \mathbf{a}_i) \qquad i = 1, 2. \tag{29d}$$

Until convergence.

Further simplification is made possible by defining $\mathbf{v}_i = \mathbf{u}_i - \mathbf{d}_i$, which gives the following result.

Initialize: $\mu > 0$, $\mathbf{d}_i$, $i = 1, 2$
Repeat

$$\mathbf{v}_i \leftarrow \left(\arg\min_{\mathbf{v}_i} \lambda_i R_i(\mathbf{v}_i + \mathbf{d}_i) + \mu\|\mathbf{v}_i - \mathbf{a}_i\|_2^2\right) - \mathbf{d}_i \quad i = 1, 2 \tag{30a}$$

$$\mathbf{c} \leftarrow \mathbf{y} - \mathbf{F}_1\mathbf{v}_1 - \mathbf{F}_2\mathbf{v}_2 \tag{30b}$$

$$\mathbf{a}_i \leftarrow \mathbf{v}_i + \frac{1}{2}\mathbf{F}_i^{\mathsf{H}}\mathbf{c} \quad i = 1, 2 \tag{30c}$$

$$\mathbf{d}_i \leftarrow \mathbf{a}_i - \mathbf{v}_i \qquad i = 1, 2. \tag{30d}$$

Until convergence.

Rearranging the terms $\mathbf{a}_i$ and $\mathbf{d}_i$ to eliminate redundant computation gives the final iterative algorithm, shown in the following.

Initialize: $\mu > 0$, $\mathbf{d}_i$, $i = 1, 2$
Repeat

$$\mathbf{v}_i \leftarrow \left(\arg\min_{\mathbf{v}_i} \lambda_i R_i(\mathbf{v}_i + \mathbf{d}_i) + \mu\|\mathbf{v}_i - \mathbf{a}_i\|_2^2\right) - \mathbf{d}_i \quad i = 1, 2 \tag{31a}$$

$$\mathbf{c} \leftarrow \mathbf{y} - \mathbf{F}_1\mathbf{v}_1 - \mathbf{F}_2\mathbf{v}_2 \tag{31b}$$

$$\mathbf{d}_i \leftarrow \frac{1}{2}\mathbf{F}_i^{\mathsf{H}}\mathbf{c} \qquad i = 1, 2 \tag{31c}$$

$$\mathbf{a}_i \leftarrow \mathbf{d}_i + \mathbf{v}_i \quad i = 1, 2. \tag{31d}$$

Until convergence.

We have proposed that WTC and weather be obtained by solving (9) with

$$\mathbf{F}_1 = \mathbf{I} \tag{32a}$$

$$R_1(x) = \sum_n |x(n+1) - x(n)| \tag{32b}$$

$$R_2(x) = \sum_n \left[\sum_k^{K-1} |x(n+k)|^2 \right]^{\frac{1}{2}}. \tag{32c}$$

Here, the function $R_1(\cdot)$ promotes the sparsity of the first derivative of the input signal [26]. The penalty function $R_2(\cdot)$ is the OGS function which promotes group sparsity, where K defines the group size [24].

The subminimization problem in (31a) for $i = 1$ can be rewritten by substituting the TV in place of R_1, shown as

$$\mathbf{v}_1 \leftarrow \left(\arg\min_{\mathbf{v}_1} \lambda_1 \sum_n |v_1(n+1) - v_1(n) + d_1(n+1) - d_1(n)| + \mu \|\mathbf{v}_1 - \mathbf{a}_1\|_2^2 \right) - \mathbf{d}_1. \tag{33}$$

Focusing on the suboptimization problem inside the parenthesis and introducing the new variables $\mathbf{g} = \mathbf{v}_1 + \mathbf{d}_1$ and $\mathbf{e} = \mathbf{d}_1 + \mathbf{a}_1$, the suboptimization problem can be expressed as

$$\arg\min_{\mathbf{e}} \lambda_1 \sum_n |g(n+1) - g(n)| + \mu \|\mathbf{g} - \mathbf{e}\|_2^2. \tag{34}$$

Problem (34) is a TV denoising (TVD) problem and can be solved using one of several previously developed algorithms, e.g., [26] and [40]–[44]. Substituting TVD in place of the TVD problem, (33) can be rewritten as

$$\mathbf{v}_1 \leftarrow \text{TVD}\left(\mathbf{a}_1 + \mathbf{d}_1, \frac{\lambda_1}{\mu} \right) - \mathbf{d}_1. \tag{35}$$

The subminimization problem in (31a) for $i = 2$ can be rewritten by substituting the overlapping group sparsity equalizer [see (32c)] in place of R_2, shown as

$$\mathbf{v}_2 \leftarrow \left(\arg\min_{\mathbf{v}_2} \lambda_2 \sum_n \left[\sum_k^{K-1} |\mathbf{a}_2(n+k)|^2 \right]^{\frac{1}{2}} + \mu \|\mathbf{v}_2 - \mathbf{a}_2\|_2^2 \right) - \mathbf{d}_1. \tag{36}$$

By introducing the new variables $\mathbf{h} = \mathbf{v}_2 + \mathbf{d}_2$ and $\mathbf{f} = \mathbf{d}_2 + \mathbf{a}_2$, the suboptimization problem inside the parenthesis in (36) is given by

$$\arg\min_{\mathbf{h}} \lambda_2 \sum_n \left[\sum_k^{K-1} |\mathbf{h}(n+k)|^2 \right]^{\frac{1}{2}} + \mu \|\mathbf{h} - \mathbf{f}\|_2^2. \tag{37}$$

Problem (37) is a group sparse signal denoising problem and can be solved using one of several recently developed algorithms, such as [24] and [28]. Therefore, (36) can be written as

$$\mathbf{v}_2 \leftarrow \text{OGS}\left(\mathbf{a}_2 + \mathbf{d}_2, \frac{\lambda_2}{\mu}, K \right) - \mathbf{d}_2. \tag{38}$$

The proposed method for the weather data and WTC separation problem is summarized as follows.

Initialize: $\mathbf{F}_1 = \mathbf{I}$, $\mathbf{F}_2 = \text{STFT}$, $\mu > 0$, $\mathbf{d}_i = 0$, $i = 1, 2$
Repeat

$$\mathbf{v}_1 \leftarrow \text{TVD}\left(\mathbf{a}_1 + \mathbf{d}_1, \frac{\lambda_1}{\mu} \right) - \mathbf{d}_1 \tag{39a}$$

$$\mathbf{v}_2 \leftarrow \text{OGS}\left(\mathbf{a}_2 + \mathbf{d}_2, \frac{\lambda_2}{\mu}, K \right) - \mathbf{d}_2 \tag{39b}$$

$$\mathbf{c} \leftarrow \mathbf{y} - \mathbf{F}_1\mathbf{v}_1 - \mathbf{F}_2\mathbf{v}_2 \tag{39c}$$

$$\mathbf{d}_i \leftarrow \frac{1}{2}\mathbf{F}_i^{\mathsf{H}}\mathbf{c}, \qquad i = 1, 2 \tag{39d}$$

$$\mathbf{a}_i \leftarrow \mathbf{d}_i + \mathbf{v}_i, \qquad i = 1, 2. \tag{39e}$$

Until convergence.

Note that we initialize $\mathbf{d}_i = \mathbf{0}$, but the algorithm is globally convergent regardless of the initialization. Proposed approach (39) can be implemented, as shown in Table I.

REFERENCES

[1] "U.S. wind industry first quarter 2014 market report," Amer. Wind Energy Assoc. (AWED), Washington, DC, USA, Tech. Rep., AWEA Data Services, Apr. 2014.

[2] M. M. Butler and D. A. Johnson, "Feasibility of mitigating the effects of wind farms on primary radar," Tech. Rep. W/14/00623/REP, Alenia Marconi Syst. Ltd., Portsmouth, U.K., Jun. 2003.

[3] H. Ling *et al.*, "Assessment of offshore wind farm effects on sea surface, subsurface and airborne electronic systems," Tech. Rep. DE-EE0005380, Univ. Texas, Austin, TX, USA, Aug. 30, 2013.

[4] "The Effect of windmill farms on military readiness," Tech. Rep. ADA-455993, Office Director Defense Res. Eng., Washington, DC, USA, 2006.

[5] J. Perry and A. Biss, "Wind farm clutter mitigation in air surveillance radar," in *Proc. IEEE Radar Conf.*, Apr. 2007, pp. 93–98.

[6] F. Uysal, U. Pillai, I. Selesnick, and B. Himed, "Signal decomposition for wind turbine clutter mitigation," in *Proc. IEEE Radar Conf.*, May 2014, pp. 60–63.

[7] R. J. Vogt *et al.*, "An update on policy considerations of wind farm impacts on WSR-88D operations," in *Proc. 24th Int. Conf. Interactive Inf. Process. Syst. Meteorol., Oceanogr., Hydrol.*, 2008, pp. 1–11.

[8] D. W. Burgess, T. Crum, and R. Vogt, "Impacts of wind farms on WSR-88D radars," in *Proc. 24th Int. Conf. Interactive Inf. Process. Syst. Meteorol., Oceanogr., Hydrol.*, 2008, pp. 1–16.

[9] B. Isom *et al.*, "Detailed observations of wind turbine clutter with scanning weather radars," *J. Atmos. Ocean. Technol.*, vol. 26, no. 5, pp. 894–910, 2009.

[10] J. Zheng, B. Perfetti, M. Kaveh, S. Bachmann, and R. Monson, "Azimuth-frequency analysis for wind farm clutter identification and mitigate on in Doppler weather radars," in *Proc. 35th Conf. Radar Meteorol.*, 2011, pp. 1–15.

[11] B. Perfetti, J. Zheng, and M. Kaveh, "Signal processing for wind turbine interference mitigation in Doppler weather radars: Data synthesis, clutter detector performance, and spectral interpolation in range-azimuth-Doppler," in *Proc. IET Int. Conf. Radar Syst.*, Oct. 2012, pp. 1–6.

[12] F. Nai, S. Torres, and R. Palmer, "On the mitigation of wind turbine clutter for weather radars using range-Doppler spectral processing," *IET Radar, Sonar Navigat.*, vol. 7, no. 2, pp. 178–190, Feb. 2013.

[13] F. Kong, Y. Zhang, and R. Palmer, "Impacts of wind turbine siting on radar clutter mitigation," in *Proc. IET Int. Radar Conf.*, Apr. 2013, pp. 1–5.

[14] F. Kong, Y. Zhang, and R. Palmer, "Wind turbine clutter mitigation for weather radar by adaptive spectrum processing," in *Proc. IEEE RADAR*, May 2012, pp. 471–474.

[15] M. Farshchian and I. Selesnick, "Application of a sparse time-frequency technique for targets with oscillatory fluctuations," in *Proc. Int. WDD*, Jan. 2012, pp. 191–196.

[16] I. W. Selesnick, K. Y. Li, S. U. Pillai, and B. Himed, "Doppler-streak attenuation via oscillatory-plus-transient decomposition of IQ data," in *Proc. IET Int. Conf. Radar Syst.*, 2012, pp. 1–4.
[17] F. Uysal, I. Selesnick, U. Pillai, and B. Himed, "Dynamic clutter mitigation using sparse optimization," *IEEE Aerosp. Electron. Syst. Mag.*, vol. 29, no. 7, pp. 37–49, Jul. 2014.
[18] S. Nguyen and W. Al-Ashwal, "Sea clutter mitigation using resonance-based signal decomposition," *IEEE Geosci. Remote Sens. Lett.*, vol. 12, no. 11, pp. 2257–2261, Nov. 2015.
[19] S. M. Torres and D. S. Zrnic, "Ground clutter canceling with a regression filter," *J. Atmos. Ocean. Technol.*, vol. 16, pp. 1364–1372, Oct. 1999.
[20] A. Siggia and R. Passarelli, Jr, "Gaussian Model Adaptive Processing (GMAP) for improved ground clutter cancellation and moment calculation," in *Proc. ERAD*, 2004, pp. 67–73.
[21] D. S. Zrnic, "Simulation of weatherlike Doppler spectra and signals," *J. Appl. Meteorol.*, vol. 14, pp. 619–619, Jun. 1975.
[22] "Doppler radar meteorological observations: Part C WSR-88D products and algorithms. Federal meteorological handbook no. 11," Tech. Rep. FCM-H11C-2006, Off. Fed. Coord. Meteorol. Serv. Support. Res., Silver Spring, MD, USA, Apr. 5–13, 2006, pp 5–11.
[23] J.-L. Starck, Y. Moudden, J. Bobina, M. Elad, and D. Donoho, "Morphological component analysis," in *Proc. SPIE Wavelets XI*, 2005, vol. 5914, pp. 9–19.
[24] P.-Y. Chen and I. W. Selesnick, "Translation-invariant shrinkage/thresholding of group sparse signals," *Signal Process.*, vol. 94, pp. 476–489, 2014.
[25] L. I. Rudin, "Images, numerical analysis of singularities and shock filters," M.S. thesis, Dept. Comput. Sci., California Inst. Technol., Pasadena, CA, USA, 1987.
[26] L. I. Rudin, S. Osher, and E. Fatemi, "Nonlinear total variation based noise removal algorithms," *Phys. D, Nonlinear Phenom.*, vol. 60, no. 14, pp. 259–268, Nov. 1992.
[27] F. Bach, R. Jenatton, J. Mairal, and G. Obozinski, "Structured sparsity through convex optimization," Tech. Rep. HAL 00621245, French Inst. Res. Comput. Sci. Autom., Paris, France, 2011.
[28] P.-Y. Chen and I. Selesnick, "Group-sparse signal denoising: Non-convex regularization, convex optimization," *IEEE Trans. Signal Process.*, vol. 62, no. 13, pp. 3464–3478, Jul. 2014.
[29] C. Chen, Z. Peng, and J. Huang, "O(1) algorithms for overlapping group sparsity," in *Proc. 22nd ICPR*, Aug. 2014, pp. 1645–1650.
[30] I. Selesnick, "The short-time Fourier transform and speech denoising," Connexions, 2009. [Online]. Available: http://cnx.org/content/m32294
[31] B. Isom *et al.*, "Characterization and mitigation of wind turbine clutter on the WSR-88D network," in *Proc. 33rd Conf. Radar Meteorol.*, 2007.
[32] K. Hood, S. Torres, and R. Palmer, "Automatic detection of wind turbine clutter for weather radars," *J. Atmos. Ocean. Technol.*, vol. 27, pp. 1868–1880, Jul. 2010.
[33] " Doppler radar meteorological observations: Part B doppler radar theory and meteorology. Federal meteorological handbook no. 11," Tech. Rep. FCM-H11C-2006, Off. Fed. Coord. Meteorol. Serv. Support. Res., Silver Spring, MD, USA, Appendix A.4.1 and A. 4.2, Apr. 2006.
[34] R. J. Doviak, *Doppler Radar and Weather Observations*. Mineola, NY, USA: Dover, 2006.
[35] S. Ellis, J. Hubbert, M. Dixon, and G. Meymaris, "Improving NEXRAD data: Data quality algorithm progress," FY2009, Annu. Rep., Nat. Center Atmos. Res., Boulder, CO, USA, 2009.
[36] "Jetstream," Weather Glossary, Nat. Weather Service, Fort Worth, TX, USA. [Online]. Available: http://www.srh.noaa.gov/jetstream/index.htm
[37] M. V. Afonso, J. M. Bioucas-Dias, and M. A. T. Figueiredo, "Fast image recovery using variable splitting and constrained optimization," *IEEE Trans. Image Process.*, vol. 19, no. 9, pp. 2345–2356, Sep. 2010.
[38] S. Boyd, N. Parikh, E. Chu, B. Peleato, and J. Eckstein, "Distributed optimization and statistical learning via the alternating direction method of multipliers," *Found. Trends Mach. Learn.*, vol. 3, no. 1, pp. 1–122, 2011.
[39] J. Eckstein and D. P. Bertsekas, "On the Douglas–Rachford splitting method and the proximal point algorithm for maximal monotone operators," *Math. Program.*, vol. 55, pp. 293–318, 1992.
[40] A. Chambolle, "An algorithm for total variation minimization and applications," *J. Math. Imaging Vis.*, vol. 20, no. 1/2, pp. 89–97, Jan. 2004.
[41] T. Chan, S. Osher, and J. Shen, "The digital TV filter and nonlinear denoising," *IEEE Trans. Image Process.*, vol. 10, no. 2, pp. 231–241, Feb. 2001.
[42] P. Rodriguez and B. Wohlberg, "Efficient minimization method for a generalized total variation functional," *IEEE Trans. Image Process.*, vol. 18, no. 2, pp. 322–332, Feb. 2009.
[43] Y. Wang, J. Yang, W. Yin, and Y. Zhang, "A new alternating minimization algorithm for total variation image reconstruction," *SIAM J. Imaging Sci.*, vol. 1, no. 3, pp. 248–272, Jul. 2008.
[44] M. Zhu, S. Wright, and T. Chan, "Duality-based algorithms for total-variation-regularized image restoration," *Comput. Optim. Appl.*, vol. 47, no. 3, pp. 377–400, Nov. 2010.

Faruk Uysal (S'08–M'11) received the B.S. degree in electrical and electronic engineering from the University of Gaziantep, Gaziantep, Turkey, in 2008 and the M.S. and Ph.D. degrees in electrical engineering, with concentration on signal processing, from New York University, Brooklyn, NY, USA, in 2011 and 2016, respectively.

Between 2011 and 2014, he was a Staff Engineer with C&P Technologies, Inc., Closter, NJ, USA, and worked on various projects related to radar signal processing from Department of Defense agencies. Since May 2014, he has been a Radar Engineer with the Advanced Radar Research Center, The University of Oklahoma, Norman, OK, USA. His current research interests include radar signal processing, waveform design, beamforming, radar image formation, compress sensing, and inverse problems.

Ivan Selesnick (S'91–M'98–SM'08) received the B.S., M.E.E., and Ph.D. degrees from Rice University, Houston, TX, USA in 1990, 1991, and 1996, respectively, all in electrical engineering.

In 1997, he was a Visiting Professor with the University of Erlangen-Nuremberg, Erlangen, Germany. He then joined the Department of Electrical and Computer Engineering, Tandon School of Engineering, New York University (then Polytechnic University), Brooklyn, NY, USA, where he is currently a Professor. His research interests are in the areas of digital signal and image processing, wavelet-based signal processing, sparsity techniques, and biomedical signal processing.

Prof. Selesnick has been an Associate Editor of the IEEE TRANSACTIONS ON IMAGE PROCESSING, the IEEE SIGNAL PROCESSING LETTERS, and the IEEE TRANSACTIONS ON SIGNAL PROCESSING.

Bradley M. Isom (S'10–M'12) received the B.S. degree in computer engineering from the University of Nebraska, Lincoln, NE, USA, in 2005 and the M.S. and Ph.D. degrees in electrical and computer engineering from The University of Oklahoma (OU), Norman, OK, USA, in 2007 and 2012, respectively.

During his time at OU, his research interests included wind turbine clutter characterization and mitigation and advanced array and signal processing techniques. He also led the development of the Atmospheric Imaging Radar, a mobile X-band imaging radar system designed for collecting high-resolution meteorological data. He is currently a Radar Engineer with Pacific Northwest National Laboratory (PNNL), Richland, WA, USA, and works in support of the Atmospheric Radiation Measurement (ARM) radar instrumentation and infrastructure. He is responsible for developing and maintaining the ARM radar assets, as well as ensuring the delivery of quality data to end users, at PNNL. His current research interests include the identification and mitigation of dynamic clutter, the development of advanced signal and array processing techniques, and designing novel remote sensing platforms for atmospheric studies.

Dr. Isom is a member of the American Meteorological Society. He is also a member of Tau Beta Pi and Eta Kappa Nu honor societies.